The E1784K Mutation in SCN5A and Phenotypic Overlap of Type 3 Long QT Syndrome and Brugada Syndrome: A Simulation Study

KQ Wang[1], YF Yuan[1,2], S Kharche[2], H Zhang[2]

[1]School of Computer Science and Technology, Harbin Institute of Technology, Harbin, China
[2]Biological Physics Group, University of Manchester, Manchester, UK

Abstract

The E1784K mutation in SCN5A was reported as a phenotypic overlap between the Type 3 Long QT syndrome (LQT3) and the Brugada syndrome (BrS). However it is still unclear if the E1784K mutation-induced changes at ionic channel level is sufficient to account for the two phenotypic and how they affect ventricular excitation waves at tissue level. In this study, we used a biophysically detailed computer model to underpin the functional impacts of the E1784K mutation on ventricular action potential (AP), abnormal ECG and arrhythmic genesis. The simulation results suggested that augmented transmural heterogeneity of APD and ERP under the E1784K mutation condition aggravates arrhythmia risks. The E1784K mutation is insufficient to produce the phenotypic overlap between LQT3 and BrS, which may arise from a combined action of the mutation-induced changes in sodium channel currents and possible increase of I_{To} or decrease of I_{CaL} as seen in BrS.

1. Introduction

LQT3 and BrS are two distinctive hereditary cardiac diseases that present different characteristics in clinical ECG records. The hallmark of LQT3 is abnormal prolongation of QT interval and torsades de pointers, whereas BrS shows a ST segment elevation in the right precordial leads. However, some phenotypic overlaps between LQT3 and BrS were observed in patients with the SCN5A mutations such as 1795insD, E1784K and ΔKPQ. ECGs of these mutations carriers showed features of both LQT3 and BrS [1, 2]. Importantly, Class IC drugs in the overlap phenotype shorten QT interval but exacerbate the ST segment elevation and thus enhance arrhythmia risks [2, 3]. It is still unclean whether the observed SCN5A mutation is sufficient to account for the overlap phenotype and how they are pro-arrhythmic. In this study, the E1784K mutation, a most prevalent phenotypic overlap between LQT3 and BrS, was employed to address this question. We used biophysically detailed computer model to underpin the functional impacts of the E1784K mutation on transmural ventricular excitation, morphology of ECG and vulnerability of tissue to unidirectional conduction block leading to re-entrant excitation.

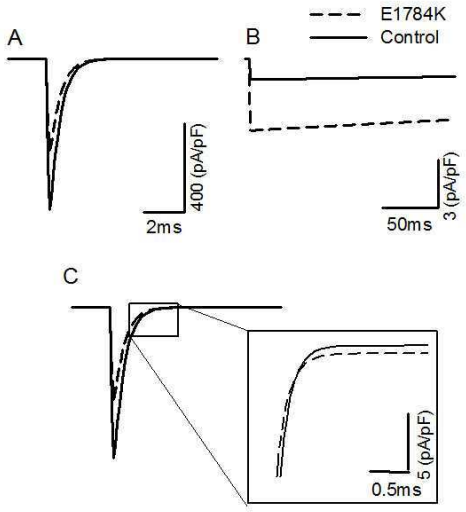

Figure 1. Simulated time trace of INa current (A), INaL current (B), and INa + INaL current (C) in 'Control' (solid line) and E1784K mutation (dashed line) conditions under a voltage-clamp experiment. Membrane potential is stepped from a holding potential -140 mV to a test potential of -20 mV. Magnification of INa + INaL current during the late phase of voltage-clamp simulation shown in square area of plane C for 'Control' and E1784K conditions.

2. Methods

The ten Tusscher et al. models [4], popular human ventricular computational models including epicardial (EPI), midmyocaridal (M) and endocardial (ENDO) cells, were modified to integrate a new formulation for the late

sodium current (I_{NaL}) [5]. To simulate E1784K mutation, experimental data of Makita et al. [1] and Wei et al. [6] on the mutation-induced changes on I_{Na} and I_{NaL} channel currents were incorporated into these models. These mutation-induced changes included a decrease in the transient I_{Na} current density by 40%, a slow down of its inactivation process by 200% and an increase in the current density of I_{NaL} by 3.5 folds. Single cell models were then incorporated into a one-dimensional multi-cellular tissue model of transmural human ventricular strand with a total length of 15 mm, which was classified as regions of EPI, M and ENDO cells with length ratio of 25:35:40. The 1D model was used to simulate conduction and propagation of ventricular excitation waves across the strand, from which the pseudo-ECG was reconstructed by using the method of Zhang et al. [7].

The mathematical method of excitation wave propagation in the strand model was described by the following partial ordinary equation:

$$\frac{\partial V_m}{\partial t} = -\frac{(I_{ion} + I_{stim})}{C_m} + D \cdot \nabla V_m \qquad (1)$$

where V_m is the cellular transmembrane potential, C_m is the capacitance, and D is the diffusion coefficient modelling intracellular electrical coupling. I_{ion} is the total ionic current density from the ventricular cell models. I_{stim} is the external stimulus current.

The pseudo-ECG was computed as an integral of spatial gradient of membrane potential at all positions on the strand from a virtual electrode located in the extracellular space.

$$\phi_e = \frac{a^2 \cdot \delta}{4} \int (-\nabla V_m) \cdot \nabla \frac{1}{x - x_0} dx \qquad (2)$$

where ϕ_e represents the unipolar potential recorded at an electrode 2 cm (x_0) from the epicardial end of the strand, δ is the ratio of the extra- and intra-cellular conductivities. a is the radius of the fibre and $|x\text{-}x_0|$ is the distance from the electrode to any point in the strand.

3. Results

Figure 1 shows the simulated sodium currents of both 'Control' and the E1784K mutation conditions under the voltage clamp protocol from a holding potential -140 mV to a test potential of -20 mV. Though the peak current density of transient I_{Na} current under the E1784K mutation was approximately 40% less than that in 'Control' (Fig. 1A), the I_{NaL} current of the E1784K was about 3.5 folds larger than that in 'Control' (Fig. 1B). It made a persistent increase of Na^+ influx in E1784K compared with 'Control' during the late phase of voltage-clamp simulation (Fig. 1C). The APs and values of AP duration (APD) at 90% repolarization (APD_{90}) are computed for EPI, M and ENDO cells under the two conditions respectively, as shown in Figure 2. The ionic homeostasis in myocardial cells was broken by the altered kinetics of sodium currents under the E1784K mutation (compare Fig. 2A and 2B). Increases of the I_{NaL} current and Na^+ influx significantly prolonged the plateau of APs and APD_{90} (from 285.30ms, 352.00ms and 283.64ms in 'Control' to 316.68ms, 429.04ms and 310.56ms in E1784K for ENDO, M and EPI cell types respectively, seen in Fig. 2C), and augmented transmural heterogeneity of APDs (differences between M-ENDO, M-EPI and ENDO-EPI APD_{90}s were increased from 66.70ms, 68.36ms and 1.66ms in 'Control' to 112.36ms, 118.48ms and 6.12ms in E1784K respectively, shown in Fig. 2D). Consistent with this, the E1784K mutation also enlarged transmural heterogeneity of effective refractory period (ERP). The differences between M-ENDO, M-EPI and ENDO-EPI ERPs were enhanced from 70ms, 67ms and 3ms in 'Control' to 93ms, 89ms and 4ms in E1784K at 1000ms cycle length (CL) respectively (Fig. 3).

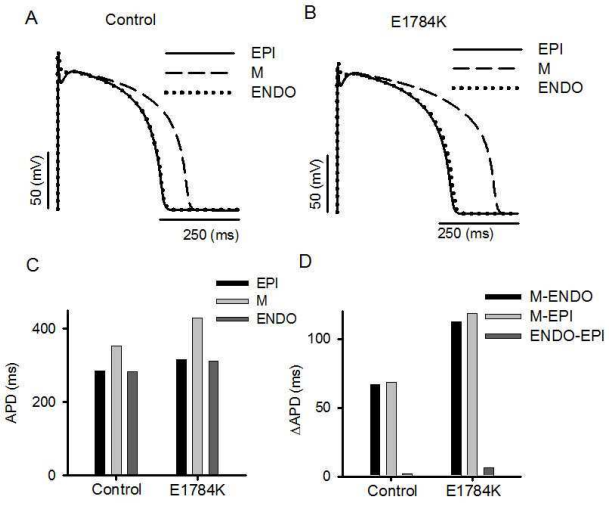

Figure 2. Computed APs of EPI, M and ENDO cells in 'Control' (A) and E1784K (B) conditions. Heterogeneous effects of the mutation in APD (C) and spatial APD dispersion (D) between the three cell types.

A 1D strand model was employed to quantify the vulnerability of tissue to unidirectional conduction block in response to a test stimulus applied to the refractory tail of a previous excitation wave for 'Control' and the E1784K mutation. Figure 4A-C show the propagation of excitation wave in the tissue (from ENDO to EPI) and the response of the tissue to a delayed test stimulus after the 50th stimulus (at pacing CL=1000ms). In Fig. 4A, a bi-directional conduction block was observed because the test stimulus was applied soon after the previous excitation and the tissue did not recover thoroughly for re-excitation. In contrast to this case, a bi-directional conduction was generated since the test stimulus was applied with a long time delay and the tissue had enough time to recover and could response to generate a next excitation. The test stimulus must be applied within a

small proper time window (vulnerable time window) after the previous excitation to produce a unidirectional conduction block, as shown in Fig.4B. The widths of vulnerable time window (VW) were computed in the tissue strand with 0.75mm space step under 'Control' and the E1784K mutation (Fig. 4D). The widths of computed VW increased more in the E1784K compared with the widths in 'Control' at the two ends of the strand as a consequence of the augmented transmural heterogeneity of APD and ERP. Hence, the E1784K mutation in SCN5A gene aggravated the vulnerability of ventricular tissue and risks of arrhythmia.

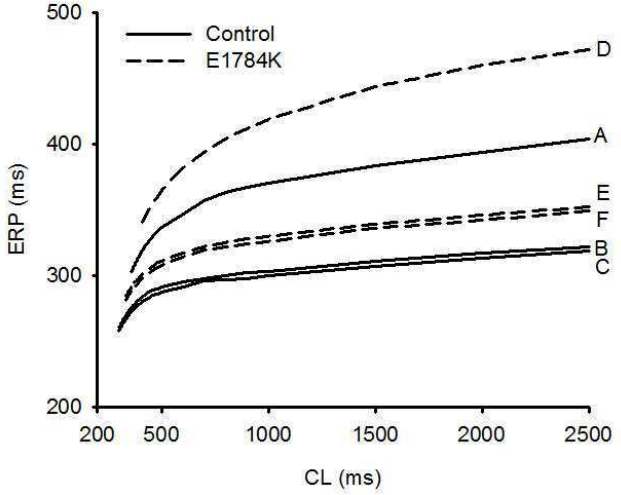

Figure 3. Rate-dependent ERPs of the three cell types under 'Control' and the E1784K mutation. A-C: (A) M cell, (B) ENDO cell and (C) EPI cell in 'Control' condition. D-F: (D) M cell, (E) ENDO cell and (F) EPI cell in E1784K.

Using the 1D strand model, pseudo-ECGs were also simulated under 'Control' and the E1784K mutation conditions. In the simulation, the pseudo-QT interval prolonged and the amplitude and width of T-wave increased (Fig. 5Bi) because of the augmented plateau and slow repolarization of AP induced by the E1784K mutation (Fig. 5Ai). The prolonged QT interval and increased T-wave are typical ECG features of LQT3. But it hasn't been observed an elevated ST segment of the ECG hallmark of BrS. The loss of AP dome within the epicardium was suggested to be the substrate of elevated ST segment in the ECG of BrS [8, 9], which are possibly due to an increase of I_{To} current and a decrease of I_{CaL} current are linked to the BrS as seen Antzelevitch et. al. [10, 11]. In dependence on the simulation study of BrS [12], the coved-type Brugada (BrS1) was modeled via increasing I_{To} current density G_{To} by 27% and shifting the half-activation potential of the r gate from 20 mV to 2.5 mV. The saddle-back type Brugada (BrS2) is simulated by reducing I_{CaL} current density G_{CaL} with 35%. Fig. 5Aii and Fig. 5Aiii show the loss of AP dome in E1784K+BrS1 and BrS1 or accentuated notch of AP in E1784K+BrS2 and BrS2. But the APDs augmented in E1784K+BrS1 and E1784K+BrS2 compared with those in BrS1 and BrS2. Therefore, hallmark of the BrS ECG in BrS1 and BrS2 is reproduced. Features of both LQT and BrS ECG are only observed in E1784K+BrS1 and E1784K+BrS2 (Fig. 5Bii and Fig. 5Biii). The simulation results suggest that the underlying genesis of phenotypic overlap of LQT3 and BrS may not be solely due to the E1784K SCN5A gene mutation, but due to a combined action of the mutation-induced changes in sodium channel currents and possible increase of I_{To} or decrease of I_{CaL}.

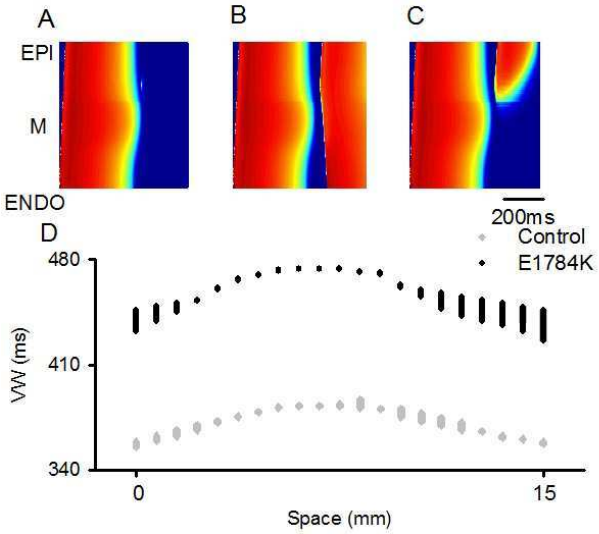

Figure 4. Space-time plot of excitation wave propagation and response of the tissue to a premature test stimulus at a local site of the strand at various time interval of delay (Δt). Space runs y-direction from the bottom (ENDO) to the top (EPI). Time runs x-direction from left to right. A-C: Test stimulus applied at EPI part (marked by the white arrow) with gradually increasing Δt. (A) Bi-directional block. (B) Unidirectional block. (C) Bi-directional conduction. (D) The begin time and time width of unidirectional block in the whole strand with the 0.75 mm space step in 'Control' and E1784K conditions.

4. Discussion and conclusions

These simulations revealed the non-uniform prolongation of APD induced by the E1784K SCN5A mutation, which augments transmural heterogeneity of ventricular repolarization that increases the vulnerability of ventricular tissue to the genesis of arrhythmia risks. It also illustrated the causative link between the mutation and LQT3. The elevated ST segment in ECGs of E1784K mutation carrier can't be sufficiently accounted for by the mutation-induced changes in I_{Na} and I_{NaL} alone. It may

arise from a combined action of the mutation-induced changes in sodium channel currents and possible increase of I_{To} and decrease of I_{CaL} as observed experimentally in BrS.

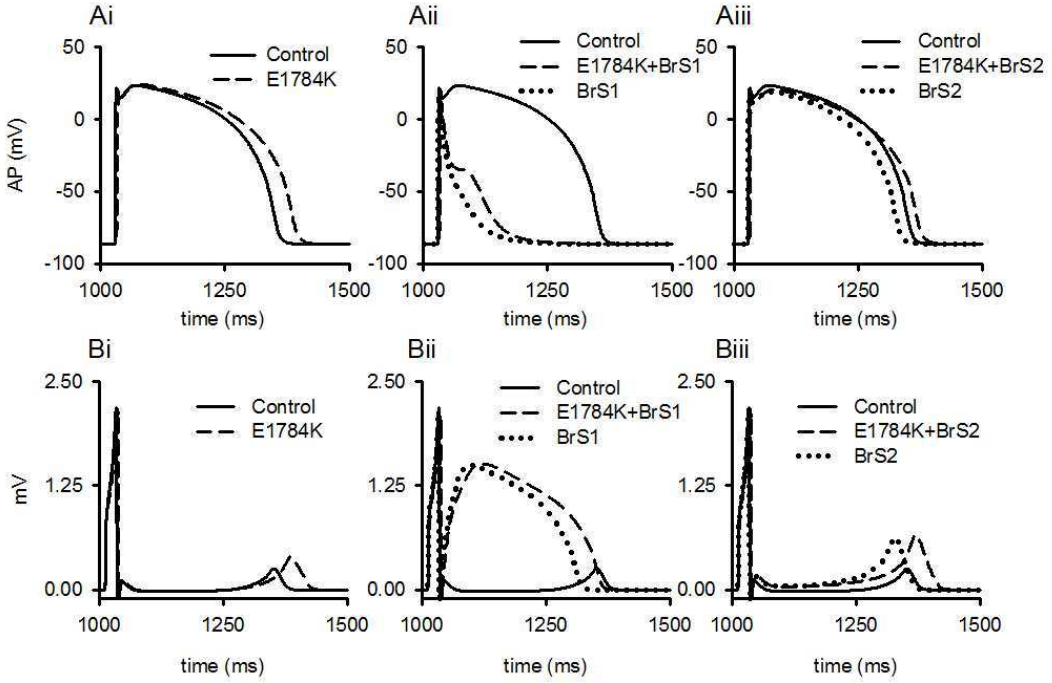

Figure 5. Computed APs of EPI cell and pseudo-ECGs in the strand model at 1 Hz pacing. Ai-iii: AP waveforms in 'Control' and E1784K conditions, in 'Control', E1784K+BrS1 and BrS1 (altered kinetics of I_{To} current) conditions and in 'Control', E1784K+BrS2 and BrS2 (partial block of I_{CaL} current) conditions. Bi-iii: simulated morphology of pseudo-ECGs.

Acknowledgements

This work was supported by two NSFC projects (grant No. 60872099 and No. 60571025), the 863 project (grant No. 2006AA01Z308) and the CSCF Scholarship (No. 8261081030002).

References

[1] Makita N, Behr E, Shimizu W et.al. The E1784K mutation in SCN5A is associated with mixed clinical phenotype of type 3 long QT syndrome. J Clin Invest. 2008;118(6): 2219-29.

[2] Remme CA, Verkerk AO, Nuyens D et.al. Overlap syndrome of cardiac sodium channel disease in mice carrying the equivalent mutation of human SCN5A-1795insD. Circulation. 2006;114(24):2584-94.

[3] Priori SG, Napolitano C, Schwartz PJ.et.al. The elusive link between LQT3 and Brugada syndrome: the role of flecainide challenge. Circulation. 2000;102(9):945-7.

[4] Ten Tusscher KH, Noble D, Noble PJ et.al. A model for human ventricular tissue. Am J Physiol Heart Circ Physiol. 2004;286(4):H1573-89.

[5] Xia L, Zhang Y, Zhang H et.al. Simulation of Brugada syndrome using cellular and three-dimensional whole-heart modeling approaches. Physiol Meas. 2006;27(11):1125-42.

[6] Wei J, Wang DW, Alings M et.al. Congenital long-QT syndrome caused by a novel mutation in a conserved acidic domain of the cardiac Na+ channel. Circulation. 1999 22;99(24):3165-71.

[7] Zhang H, Hancox JC. In silico study of action potential and QT interval shortening due to loss of inactivation of the cardiac rapid delayed rectifier potassium current. Biochem Biophys Res Commun. 2004;322(2):693-9.

[8] Benito B, Brugada R, Brugada J, Brugada P. Brugada syndrome. Prog Cardiovasc Dis. 2008;51(1):1-22.

[9] Yan GX, Antzelevitch C. Cellular basis for the Brugada syndrome and other mechanisms of arrhythmogenesis associated with ST-segment elevation. Circulation. 1999;100:1660-1666.

[10] Fish JM, Antzelevitch C. Cellular mechanism and arrhythmogenic potential of T-wave alternans in the Brugada syndrome. J Cardiovasc Electrophysiol. 2008;19: 301-308.

[11] Ten Tusscher KH, Panfilov AV. Cell model for efficient simulation of wave propagation in human ventricular tissue under normal and pathological conditions. Phys Med Biol. 2006;51(23):6141-56.

Address for correspondence

Yongfeng Yuan
No.92, West DaZhi Street, Harbin,150001,China
E-mail address : yuanyongfeng@gmail.com